Microchim Acta (2012) 178:331–340
DOI 10.1007/s00604-012-0842-1

ORIGINAL PAPER

Label-free sandwich type of immunosensor for hepatitis C virus core antigen based on the use of gold nanoparticles on a nanostructured metal oxide surface

Cuixia Ma · Guoming Xie · Wei Zhang · Mo Liang · Bei Liu · Hua Xiang

Received: 28 February 2012 / Accepted: 25 May 2012 / Published online: 9 June 2012

Abstract We report on the construction of a label-free electrochemical immunosensor for detecting the core antigen of the hepatitis C virus (HCV core antigen). A glassy carbon electrode (GCE) was modified with a nanocomposite made from gold nanoparticles, zirconia nanoparticles and chitosan, and prepared by in situ reduction. The zirconia nanoparticles were first dispersed in chitosan solution, and then AuNPs were prepared in situ on the ZrO_2-chitosan composite. In parallel, a nanocomposite was synthesized from AuNPs, silica nanoparticles and chitosan, and conjugated to a secondary antibody. The properties of the resulting nanocomposites were investigated by UV-visible photometry and transmission electron microscopy, and the stepwise assembly process was characterized by means of cyclic voltammetry and electrochemical impedance spectroscopy. An sandwich type of immunosensor was developed which displays high sensitivity to the HCV core antigen in the concentration range between 2 and 512 ng mL^{-1}, with a detection limit of 0.17 ng mL^{-1} (at S/N=3). This immunosensor provides an alternative approach towards the diagnosis of HCV.

Keywords Hepatitis C virus core antigen · Electrochemical immunosensor · AuNPs/ZrO_2-Chits nanocomposite · AuNPs/SiO_2-Chits nanocomposite

Electronic supplementary material The online version of this article (doi:10.1007/s00604-012-0842-1) contains supplementary material, which is available to authorized users.

C. Ma · G. Xie · W. Zhang · M. Liang · B. Liu · H. Xiang (✉)
Key Laboratory of Medical Diagnostics of Ministry of Education, Department of Laboratory Medicine, Chongqing Medical University,
Chongqing 400016, People's Republic of China
e-mail: xianghuacq@163.com

Introduction

Hepatitis C virus (HCV) is the major causative agent of chronic viral hepatitis which can develop into cirrhosis and hepatocellular carcinoma [1, 2]. HCV infection currently affects approximately 200 million people worldwide [3]. HCV infection develops into chronic disease in approximately 70 % patients and there was a decreased response to therapy with progression from acute to chronic infection [4]. Therefore, early detection is the key to prevent chronic infection. There are a number of diagnostic tests for hepatitis C virus infection including detection of anti-HCV antibody and quantification of HCV RNA [5, 6]. Detection of anti-HCV antibody can not distinguish between a current or past infection because people will retain anti-HCV antibodies for life once they are exposed to HCV. In addition, testing anti-HCV antibody might provide false negative results because it takes 45–68 days to develop anti-HCV antibody post HCV infection [7, 8]. On the other hand, detection of HCV RNA can distinguish between a current or past infection. However, detection of HCV RNA could provide false positive results due to contamination. It is also expensive and labor-intensive for routine use. It has been reported that HCV core antigen can be detected in the serum for most patients during the acute infection [9, 10]. HCV core antigen levels correlate well with HCV RNA levels and may consequently be an indirect marker of HCV replication as a low-cost alternative for diagnosis of HCV acute infection [11–14]. There are various methods, which can be used to detect HCV core antigen [6, 8, 10]. Among them, electrochemical immunosensors, based on the highly specific molecular recognition of antigen by its antibodies, have created a high interest in clinical diagnostics and will be expected to provide fast and highly sensitive detection of HCV

core antigen [15]. However, there is no report using any electrochemical immunosensor for detection of HCV core antigen based on our knowledge. It is valuable to explore the possibility to use electrochemical immunosensors to detect HCV core antigens for its clinical application.

The advantages of excellent sensitivity, rapid response and cost-effectiveness of the nanostructured metal-oxides make them the preferable choices to fabricate biosensor [16–18]. Among them, zirconia (ZrO_2) nanoparticles are inorganic oxides with thermal stability and chemical inertness without toxicity [19, 20]. It is suitable for the adsorption of proteins with high isoelectric point (IEP) due to the low IEP of ZrO_2 [21]. It has been reported that ZrO_2/Au nanocomposite film can be used to modify electrode. Wang et al. built ZrO_2/Au film-modified electrode as a parathion biosensor through a sol-gel procedure [22]. Zhang et al. built DNA biosensor based on ZrO_2/Au film using electrodeposit technique [23]. However, too many steps were involved in these fabrication processes. The synthesis of AuNPs using chitosan as both reducing and stabilizing agent, which was considered to be a green approach, was first described by Huang et al [24]. Since then, several researches have made an attempt and successfully reduced AuNPs onto carbon nanotubes as well as other nanomaterials. Jiang et al. reported the one-step synthesis of a nanocomposite composed of single-walled carbon nanotubes and gold nanoparticles [25]. Huang et al. synthesized AuNPs onto the multi-walled carbon nanotubes to fabricate a carcinoembryonic antigen immunosensor [26]. Wang et al. accomplished the synthesis of gold nanoparticles on surfaces of poly (dimethylsiloxane) film [27]. Nevertheless, to the best of our knowledge, the synthesis of AuNPs on the surfaces of ZrO_2 nanoparticles by chitosan in electrochemical immunosensor has not yet been reported. Hence, it is interested to apply this approach to generate immunosensor for the detection of HCV core antigens.

Silica (SiO_2) nanoparticles are robust inorganic materials, which have been used to prepare sandwich-type immunosensors due to their convenient properties including a large specific surface area, good monodispersity, perfect biocompatibility and suitability for many surface immobilization mechanism [28–30]. Lin et al. constructed a sensitive immunosensor using functionalized methylene blue/SiO_2 core-shell nanoparticle loaded with horseradish peroxidase (HRP) for BaP analysis [31]. However, the labeled antibody process and the design of signal amplification were time-consuming. There is a need to improve the process. In this experiment, AuNPs/SiO_2-Chits nanocomposite was obtained using the in situ reduction method. We used AuNPs/SiO_2-Chits nanocomposite integrated with secondary antibody (Ab_2) without labeled HRP. The AuNPs/SiO_2-Chits nanocomposite has the ability to greatly enhance the response signal for the reason: hexacyanoferrate (II) $[Fe(CN)_6]^{4-}$possesses an effective electron transferability as an electron mediator and this negatively charged mediator is expected to be firmly immobilized on the positively charged chitosan film through electrostatic interaction. This strategy not only simplifies the fabrication procedure, but also obtains high sensitivity and selectivity.

In the present study, we report the in situ synthesis of AuNPs/ZrO_2-Chits nanocomposite and AuNPs/SiO_2-Chits nanocomposite by one-step direct chemical reduction. In experiment, chitosan was used as reducing reagent and disperser. AuNPs/ZrO_2-Chits nanocomposite, modified on GCE, was used to immobilize primary HCV core antibodies. It forms sandwich-type immunosensor in combination with secondary antibody immobilized on AuNPs/SiO_2-Chits nanocomposite. The fabricated immunosensor exhibited high sensitivity, selectivity and good reproducibility for the quantification of HCV core antigen.

Experimental

Chemicals and materials

Chloroauric acid ($HAuCl_4$) and Bovine serum albumin (BSA, 96–99 %) were purchased from Sigma (St. Louis, MO, USA, http://www.sigmaaldrich.com). Chitosan (Chits, 90 %) was bought from Sangon Biotech Co. (Shanghai, China, http://www.sangon.com). ZrO_2 nanoparticles and SiO_2 nanoparticles were obtained from Shanghai ChaoWei Nanotechnology Co. (shanghai, China, http://www.cwnano.com). Hepatitis C virus core antigen and Hepatitis C virus core antibody were purchased from ViroStat (Portland, USA, http://www.virostat-inc.com). All other reagents were of at least analytical-reagent grade and all solutions were prepared using double distilled water. The working environment was 0.1 M phosphate buffer solution (pH 5.5) containing 10 mM $[Fe(CN)_6]^{3-/4-}$ and 0.1 M KCl solution.

Apparatus

Electrochemical experiments were performed on CHI660D electrochemical workstation (Shanghai Chenhua Apparatus, China, http://chi.instrument.com.cn) with a conventional three-electrode system composed of a platinum wire auxiliary electrode, a saturated calomel reference electrode (SCE) and the modified glassy carbon electrode (GCE, diameter was 3 mm) as working electrode. The sizes of synthesized AuNPs on the surfaces of ZrO_2 nanoparticles and SiO_2 nanoparticles were observed by transmission electron microscopy (TEM, Hitachi-7500, Japan, http://www.hitachi-hitec.com). The morphology and composition of ZrO_2 nanoparticles and SiO_2 nanoparticles were studied by a Nova 400 field emission scanning electron microscope (SEM, FEI Nova-400, USA, http://www.fei.com). UV–visible absorption spectras

were performed using a Nanodrop ND-1000 Spectrophotometer (UV-Vis, ND-1000, USA, http://www.nanodrop.com).

Synthesis of AuNPs/ZrO_2-Chits nanocomposite

AuNPs/ZrO_2-Chits nanocomposite was synthesized according to the preparation procedures for carbon nanotube/gold nanoparticle composites [24–27, 32]. Chitosan solution (0.5 wt. %) were prepared by dissolving chitosan powder in 1.0 % (v/v) acetic acid solution with magnetic stirring at room temperature. The mixture was stored for about 3 days until a uniform and clear solution was obtained owing to the poor solubility of chitosan. Then a total of 1 mg of ZrO_2 nanoparticles was dispersed in 1 mL of chitosan solution following by 2 h ultrasonication to obtain an ivory homogeneous ZrO_2-Chits suspension. Finally, an aqueous solution of $HAuCl_4$ (0.5 mL, 1 mM) was added to the ZrO_2-Chits suspension under vigorous stirring for 15 min at room temperature, and then the mixture was incubated at 80 °C for approximately 1 h with stirring until the solution turned to stable pink color.

Preparation of Ab_2/AuNPs/SiO_2-Chits bioconjugate

The preparation procedure of synthesizing AuNPs/SiO_2-Chits nanocomposite was similar to the one used to make AuNPs/ZrO_2-Chits nanocomposite above except using 1 mg of SiO_2 verses 1 mg of ZrO_2. Once AuNPs/SiO_2-Chits nanocomposite was ready, the mixture was centrifuged at 4000 rpm for 10 min and washed three times with phosphate buffer solution to remove unbound AuNPs. The resulting nanocomposite was redispersed in 1.0 mL phosphate buffer solution containing 50 μL of 1 mg ml^{-1} Ab_2 overnight at 4 °C. After centrifugation, 0.25 % BSA was added to the obtained nanocomposites and incubated for 10 h to block possible remaining active sites on the AuNPs and avoid the nonspecific adsorption [33, 34]. Finally, the bioconjugate was washed with phosphate buffer solution and resuspended in 1.0 mL phosphate buffer solution containing 0.1 % BSA as secondary antibody layer.

Fabrication of the immunosensor

Before modification, the GCE with a diameter of 3 mm was polished with 1.0, 0.3 and 0.05 μm alumina slurry sequentially to remove organic matter until a mirror-like surface was obtained, and then rinsed thoroughly with double distilled water followed by ethanol under 10 min ultrasonication for each. After dried at room temperature, 5 μL AuNPs/ZrO_2-Chits nanocomposites were dropped on the pretreated electrode and left to dry at room temperature for about 15 min. The AuNPs/ZrO_2-Chits-modified electrode was then immersed into 50 μL of 1 mg mL^{-1} Ab_1 solution overnight at 4 °C. Next, the resulting electrode was washed with phosphate buffer solution to remove the physically absorbed Ab_1, and incubated with 0.25 % BSA for 1 h at 37 °C to block possible remaining active sites against nonspecific adsorption and stored at 4 °C until use.

Electrochemical measurements

For detection, the immunosensor was incubated with 0.1 M phosphate buffer solution containing different concentration of HCV core antigen for 30 min at 37 °C and then washed with phosphate buffer solution. Subsequently, the electrode was incubated with 50 μL of Ab_2/AuNPs/SiO_2-Chits bioconjugate solution for 30 min at 37 °C and then washed with phosphate buffer solution to remove nonspecifically bound conjugates. The fabrication procedures for the immunosensor and measurement procedure are illustrated in Scheme 1.

The possible application of the immunosensor in clinic analysis was investigated. Blood specimens were gifted by the First Affiliated Hospital, Chongqing Medical University and the First People's Hospital, Jiulongpo District of Chongqing. The spontaneous coagulation of blood samples in plain tubes was allowed at room temperature until serum obtained. The serum was then kept frozen in small aliquots at −20 °C. Immediately before performing the immunosensor assay, samples were thawed.

Results and discussion

Characterization

The morphologies of ZrO_2-Chits and SiO_2-Chits were characterized using scanning electron microscopy (SEM). As shown in Fig. 1a, ZrO_2-Chits nanoparticles displayed smooth morphology with diameter of about 100 nm as indicated by solid arrow. The bigger white grains were the agglomerated ZrO_2 deposit, which were

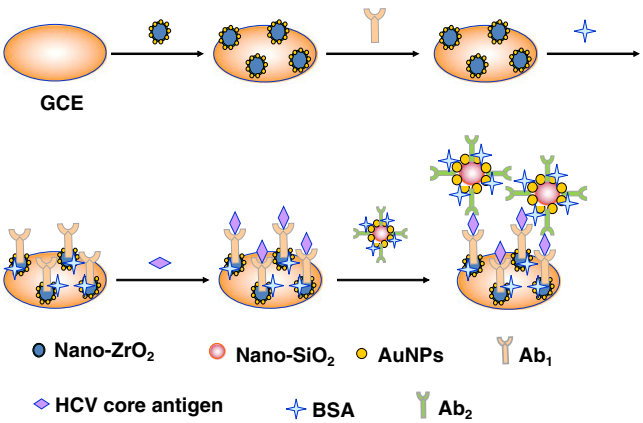

Scheme 1 Schematic illustration of the immunosensor construction process

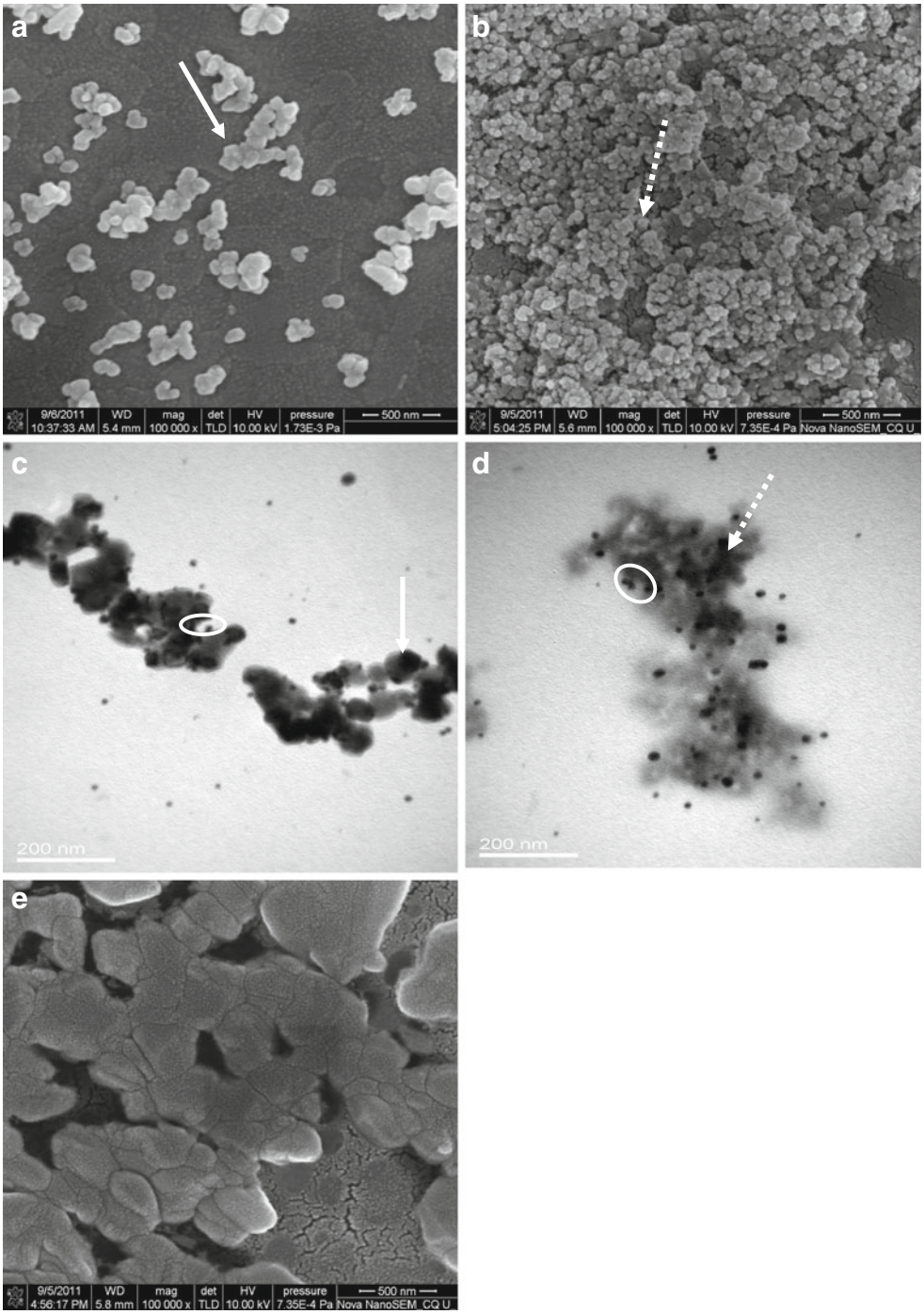

Fig. 1 The sizes and morphologies of namocomposites. SEM images of **a** ZrO_2 nanoparticles, **b** SiO_2 nanoparticles, **e** Ab_1/AuNPs/ZrO_2-Chits. TEM images of **c** AuNPs/ZrO_2-Chits nanocomposite, **d** AuNPs/SiO_2-Chits nanocomposite

from the aggregation of hydrophilic ZrO_2 in the presence of hydrophobic chitosan [35]. Figure 1b is a typical SEM photograph of SiO_2-Chits nanoparticles with the size range of 40–50 nm as indicated by dotted arrow. Transmission electron microscopy (TEM) was used to investigate the microstructures of AuNPs/ZrO_2-Chits nanocomposites (Fig. 1c) and AuNPs/SiO_2-Chits nanocomposites (Fig. 1d). As it can be seen from Fig. 1c, after AuNPs were successfully synthesized, numerous individual small dark nanoparticles were observed. The average size of AuNPs was about 20 nm as indicated by solid circle, which was smaller than ZrO_2 nanoparticles as indicated by solid arrow. AuNPs preferentially attached to the surfaces of ZrO_2 nanoparticles without exception. The formed AuNPs/ZrO_2-Chits film with two-dimension structure provided a microenvironment and lots of binding for efficient combination of biomolecules. AuNPs were indicated by solid circle and SiO_2 nanoparticles were indicated by dotted arrow in Fig. 1d. It is observed that AuNPs were successfully attached on SiO_2 nanoparticles. The morphologies

of nanocomposites with immobilized anti-HCV core antibodies are shown in Fig. 1e and the size of the antibody immobilized nanocomposites are different from ZrO_2 nanoparticles alone (Fig. 1a).

To get further insight into the formation of gold nanoparticles, UV-vis measurements were performed with a range of wavelength from 300 to 650 nm (Fig. 2). No visible adsorption peaks were observed for chitsoan solution and ZrO_2-Chits solution, respectively (Fig. 2a and c). However, the AuNPs/Chits solution exhibited an absorption peak at 520 nm (Fig. 2b), which was attributable to the typical surface plasmon resonance of AuNPs. A new absorption peak was recorded for AuNPs/ZrO_2-Chits around 535 nm (Fig. 2d), suggesting that AuNPs were successfully synthesized in the presence of ZrO_2 nanoparticles. The shift of the surface plasmon spectra of the AuNPs/ZrO_2 nanocomposites could be observed clearly. The reason is that the strong interfacial coupling between AuNPs and ZrO_2 results in electrons transfer from AuNPs to ZrO_2 during the formation of AuNPs/ZrO_2 nanocomposites [36]. It is confirmed that AuNPs/ZrO_2 is not a simple superposition of the characteristic absorptions of ZrO_2 and AuNPs. The inset graph in Fig. 2 showed that the adsorption peaks of SiO_2-Chits (Fig. 2e) and AuNPs/SiO_2-Chits nanocomposite (Fig. 2f).

Cyclic voltammetry(CV) of the nanocomposites on GCE with different processes were presented in Fig. 3. The CVs were shown in the potential range of −0.2 to 0.8 V (vs. SCE) in 10 mM $[Fe(CN)_6]^{3-/4-}$ containing 0.1 M KCl solution (pH 5.5) at a scan rate of 50 mV s^{-1}. As expected, there was an obvious increase in voltammetric signal after ZrO_2-Chits immobilized on electrode (Fig. 3a vs. f). A well-defined redox peaks was observed with the formal potential of 0.29 V and the peak to peak separation was 130 mV for the redox reaction of $[Fe(CN)_6]^{3-/4-}$at the ZrO_2-Chits film modified GCE. When the GCE was modified with AuNPs/

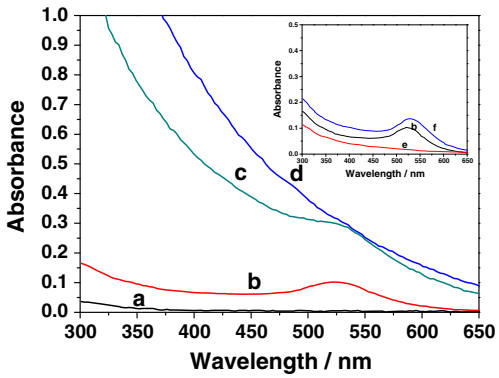

Fig. 2 UV-vis profiles of namocomposites. **a** Chits, **b** AuNPs/Chits, **c** AuNPs/ZrO_2-Chits nanocomposite, **d** ZrO_2-Chits. The inset shows SiO_2 nanoparticles: **e** SiO_2-Chits and **f** AuNPs/SiO_2-Chits nanocomposite as well as **b** AuNPs/Chits

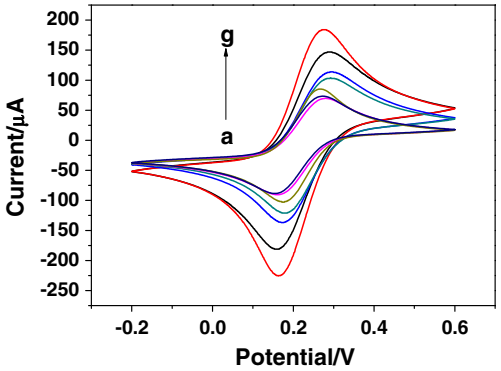

Fig. 3 Cyclic voltammograms of **a** bare GCE, **b** HCV core antigen/BSA/Ab_1/AuNPs/ZrO_2-Chits, **c** Ab_2/AuNPs/SiO_2-Chits/HCV core antigen/BSA/Ab_1/AuNPs/ZrO_2-Chits, **d** BSA/Ab_1/AuNPs/ZrO_2-Chits, **e** Ab_1 /AuNPs/ZrO_2-Chits, **f** ZrO_2-Chits, **g** AuNPs/ZrO_2-Chits. The scanning rate was 50 mV·s^{-1}

ZrO_2-Chits nanocomposites, the peak current increased greatly (Fig. 3g). The interaction between chitosan and AuNPs, which involved the electrostatic attraction between metal anions and protonated amine groups, made a great contribution in improving current signal. After immobilization of Ab_1 on the electrode surface, the membrane of Ab_1/AuNPs/ZrO_2-Chits became less conduction (Fig. 3e). The peak current further decreased after that BSA was used to block possible remaining active sites (Fig. 3d). When the immunosensor was incubated with HCV core antigen solution, the peak current decreased significantly (Fig. 3b). Anti-HCV/HCV immunocomplex might further hinder the diffusion of ferricyanide towards the electrode surface as the inert electron and mass transfer blocking layer. However, after incubating with Ab_2/AuNPs/SiO_2-Chits bioconjugate, the redox peaks increased slightly compared to Ag/BSA/Ab_1/AuNPs/ZrO_2-Chits modified electrode because AuNPs/SiO_2-Chits nanocomposites increased the electron-transfer efficiency (Fig. 3c) and acted as an efficient conducting medium between the electrode surface and electrolyte solution [37]. The construction of nanoparticles modified electrode surface was also investigated by CV. From Fig. S1 (Electronic Supplementary Material, ESM), we can see that the peak current of AuNPs/SiO_2-Chits nanocomposite (Fig. S1-f) was the highest current among AuNPs/Chits, ZrO_2/Chits, SiO_2-Chits, AuNPs/SiO_2-Chits nanocomposite and AuNPs/ZrO_2-Chits nanocomposite. It indicated that more AuNPs attached on SiO_2 nanoparticles than ZrO_2 nanoparticles. The high combination rate of AuNPs on the surface of SiO_2 nanoparticles was attributed to the high specific surface area of SiO_2 nanoparticles.

The influence of scan rate on the current response of the immunosensor was also investigated and the data was presented in Figure 4. The anodic and cathodic peak currents increased with the increment of the scan rate

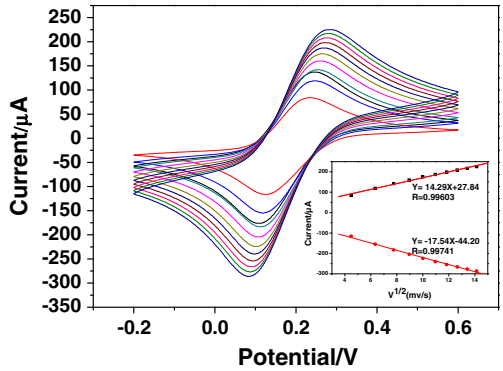

Fig. 4 Cyclic voltammograms of the immunosensor at different scan rates (from inner to outer): 20, 40, 60, 80, 100, 120, 140, 160, 180 and 200 mV.s^{-1} in 0.1 M phosphate buffer solution (pH 5.5) containing 10 mM $[Fe(CN)_6]^{3-/4-}$ and 0.1 M KCl. Inset: plot of peak currents vs the square root of scan rates

from 20 to 200 mV·s^{-1}. From the inset of Fig. 4, linear relationships with almost perfect correlation coefficients were observed between the peak currents and the square root of scan rate, suggesting that the reaction was diffusion controlled redox process. The peak-to-peak separation remained almost constant for scan rates between 20 and 200 mV·s^{-1}, indicating that electron transfer between the surface-immobilized species and the electrode surface was fast relative to the scan rate.

Electric impedance spectroscopy (EIS) is a valuable and convenient tool to monitor the interface properties of surface-modified electrodes [38]. In the Nyquist diagram, the semicircle diameter in the impedance spectrum equals the electron-transfer resistance (Ret). This resistance controls the electron-transfer kinetics of the redox probe at the electrode interface. The characteristic EIS of different modified electrodes were illustrated in Fig. 5. It was observed

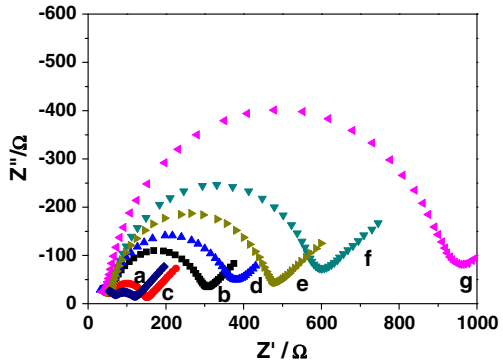

Fig. 5 EIS of different modified electrodes: **a** bare GCE, **b** ZrO_2-Chits, **c** AuNPs/ZrO_2-Chits, **d** Ab_1/AuNPs/ZrO_2-Chits, **e** BSA/Ab_1/AuNPs/ZrO_2-Chits, **f** Ab_2/HCV core antigen/BSA/Ab_1/AuNPs/ZrO_2-Chits, **g** HCV core antigen/BSA/Ab_1/AuNPs/ZrO_2 –Chits

that the bare GCE exhibited a very small semicircle (Fig. 5a). When ZrO_2-Chits were assembled, the Ret increased dramatically compared with the bare GCE (Fig. 5b), which indicated that the electrode surface generated insulating layers which functioned as barriers to the transfer of interfacial charge. After AuNPs were synthesized on ZrO_2 nanoparticles, the electrode showed a much lower resistance (Fig. 5c), implying that AuNPs/ZrO_2-Chits nanocomposite was an electric conducting material. When Ab_1 were immobilized on the modified electrode, the Ret increased which suggested that the Ab_1 had been successfully immobilized (Fig. 5d). The Ret further increased (Fig. 5e) after the electrode was blocked with BSA. Furthermore, when Ab_1/AuNPs/ZrO_2-Chits film modified electrode was incubated with HCV core antigen, the Ret increased dramatically to 900Ω (Fig. 5g), which indicated the immunocomplex layer embarrassing the electron transfer. This increase in Ret is attributed to the fact that most biological molecules are poor electrical conductors at low frequencies and cause hindrance to electron transfer. However, when Ab_2/AuNPs/SiO_2-Chits bioconjugate was loaded on HCV core antigen/BSA/Ab_1/AuNPs/ZrO_2-Chits electrode, the Ret decreased to 600Ω (Fig. 5f), indicating that Ab_2/AuNPs/SiO_2-Chits bioconjugate was helpful for signal amplification.

Optimization of experimental variables

The basic principle in electrochemical immunosensor was to preserve the protein activity and to obtain the maximal current response [39]. We selectively optimized the most important influence factors for the detection of HCV core antigen using the sandwich-type immunosensor.

First, the amperometric responses of Ab_2/SiO_2-Chits and Ab_2/AuNPs/SiO_2-Chits were compared to select the suitable nanocomposite for secondary antibody layer. Under the same conditions, Ab_2/AuNPs/ SiO_2-Chits bioconjugate induced significant higher current response at the same concentration of HCV core antigen when compared with Ab_2/SiO_2-Chits at all concentrations of HCV core antigen tested (Fig. 6). The current response increased as the concentration of HCV core antigen increase. It demonstrated that the immunosensor sensitivity could be greatly enhanced by using Ab_2/AuNPs/SiO_2-Chits bioconjugate in sandwich-type immunoassay.

Second, the optimal amount of Ab_2 used to immobilize on AuNPs/SiO_2-Chits nanocomposites was tested through using different volume (10–70 μL) of Ab_2 at same concentration (1 mg ml^{-1}). 1.5 mL of nanocomposites was redispersed in different volumes of Ab_2 overnight at 4 °C to make bioconjugates. The concentration of HCV core antigen was fixed at 256 ng mL^{-1}. The DPV peak currents increased substantially when the volume of Ab_2 increased

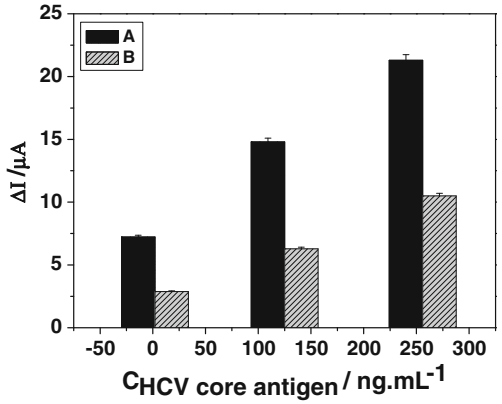

Fig. 6 Comparison of ΔI between **a** Ab_2/AuNPs/SiO_2-Chits/antigen/BSA/Ab_1/AuNPs/ZrO_2-Chits and **b** Ab_2/SiO_2-Chits/antigen/BSA/Ab_1/AuNPs/ZrO_2-Chits at different HCV antigen concentrations of 2, 64, 256 ng mL^{-1} in 10 mM $[Fe(CN)_6]^{3-/4-}$ containing 0.1 M KCl (ΔI: the increased current response when secondary antibody layer was added)

from 10 μL to 50 μL (Fig. S2, ESM). Within this volume range, the more the amount of Ab_2 combined with AuNPs/SiO_2-Chits nanocomposites, the higher the sensitivity of the electrochemical immunosensor. With further increase of volume, the obvious change was not observed. This indicated that the AuNPs/SiO_2-Chits nanocomposites reached saturation when Ab_2 over 50 μL.

Third, the effect of pH on electrochemical performance of the immunosensor was investigated using 0.1 M phosphate buffer solution with the pH range of 4.0 to 7.0 (Fig. 7a). The peak currents increased with the increasing pH value from 4.0 to 5.5 and then decreased when the pH was over 5.5. Therefore, the pH 5.5 phosphate buffer solution was selected as the detection solution.

Forth, the influence of the incubation time of Ab_1-antigen to immunoreaction was studied in the time rang of 10 to 50 min 37 °C. The peak currents increased upon the increasing incubation time and reached a platform at 30 min (Fig. 7b), indicating that 30 min is the minimal time to achieve saturated on the modified electrode. Hence, the incubation time of 30 min was used in subsequent experiments.

Last, the optimal temperature for immunoreaction was also studied in the temperature range from 15 to 50 °C. The highest peak currents can be observed at 37 °C (Fig. 7c). At this temperature, the antibody activity can be maintained at the maximum.

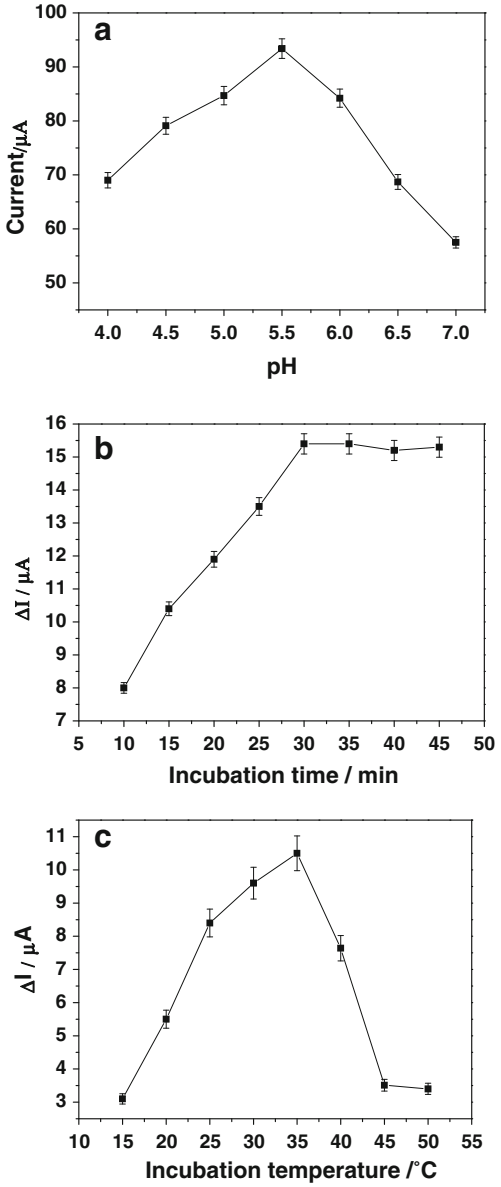

Fig. 7 Effects of (**a**) pH value of detection solution, (**b**) incubation time and (**c**) incubation temperature on CV response of the immunosensor

Performance of the immunosensor

Calibration curve was generated with different concentration of HCV core antigen to test the performance of HCV immunosersor under the optimized experimental conditions. Differential pulse voltammetrics (DPV) were determined for the amperometric response of the immunosensor in the range of 0 to 0.5 V with a pulse amplitude of 50 mV in 10 mM $[Fe(CN)_6]^{3-/4-}$ solution (pH 5.5) containing 0.1 M KCl. The calibration curve showed a good linear relationship between the peak currents and logarithm values of the analyte concentrations in the range from 2 to 512 ng mL^{-1} (Fig. 8). The linear regression equation was I=49.01+13.68log HCV core antigen with a correlation coefficient (R) of 0.99675. The detection limit was calculated to be 0.17 ng mL^{-1} at a signal-to-noise ratio of 3 (S/N=3). The current response profiles with the increase of HCV core antigen concentrations were shown in the inset of Fig. 8.

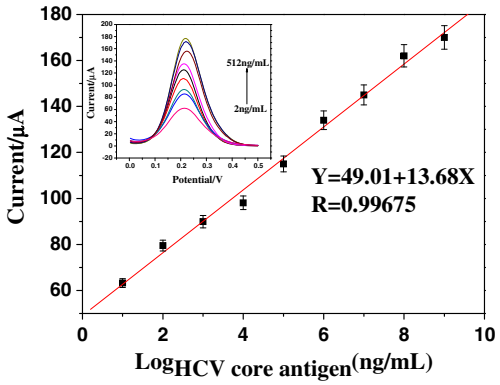

Fig. 8 Calibration curve of the immunosensor for different concentrations of HCV core antigen standard solution. Inset: differential pulse voltammetrics of the immunosensor for the detection of different concentrations of HCV core antigen in 10 mM $[Fe(CN)_6]^{3-/4-}$ containing 0.1 M KCl

The analytical performance of our HCV immunosensor has been compared to other determination methods reported (Table S1). Our immunosensor displayed a better performance than the other methods in analytical range or detection limit.

Precision, stability and selectivity of the immunosensor

To monitor the intra-assay precision of determinations, three different concentrations of HCV core antigen were repeatedly tested five times using an identical immunosensor. The relative standard deviations (RSD) of intra-assay were 5.1 %, 3.9 % and 4.8 % for 2, 32 and 128 ng mL^{-1} HCV core antigen, respectively. Meanwhile, the five immunosensors were made independently under the same conditions to estimate the inter-assay precision by measuring HCV core antigen at 8 ng mL^{-1}. The RSD was 4.2 % under this condition.

To evaluate the stability of the immunosensor,50 continuous CV measurements were carried out in working buffer at a scan rate of 50 $mV.s^{-1}$ and the RSD was 2.2 % . The immunosensor could remain about 98.5 % of the initial current response after a storage period of 30 days in the refrigerator at 4 °C with every 5 days measurement. The excellent stability of the immunosensor could be contributed by the good biocompatible property of AuNPs/ZrO_2-Chits nanocomposite with immobilized antibodies.

The selectivity of HCV core antigen immunosensor was also evaluated. The DPV peak currents had no obvious differences (Fig. S3, ESM) when 256 ng mL^{-1} of HCV core antigen was incubated with the same concentration of l-cysteine, AFP, MPO and BSA, respectively. The RSD was 3.3 %. It demonstrated that in the presence of other proteins incluidng l-cysteine, AFP, MPO, and BSA, the immunosenor displayed good specificity for the detection of HCV core antigen.

Table 1 Comparison of serum HCV core antigen levels determined using different immunoassays

Sample number	Our immunosensor ($ng{\cdot}mL^{-1}$)[a]	ELISA ($ng{\cdot}mL^{-1}$)[a]	Relative error (%)
1	4.65	4.49	3.56
2	11.47	11.71	−2.05
3	33.98	34.83	−2.44
4	64.96	60.91	6.65
5	116.72	122.03	−4.35
6	251.66	256.78	−1.99

[a] The average value of three successive determinations

Application of the immunosensors in serum samples

Six serum samples from patients were analyzed detected by our immunoassay and traditional ELISA method. The correlation results between the two methods were shown in Table 1. The measureable amount of HCV core antigen in these samples is similar as detected by two assays. The relative deviations of the proposed immunosensor were in the range of −4.35 % to 6.65 %. This experiment suggested that the immunoassay might provide a feasible alternative tool for the clinical detection of HCV core antigen in human serum.

Conclusions

We developed a novel and reliable procedure to construct label-free electrochemical immunosensor for the detection of HCV core antigen with a sandwich immunosensor. AuNPs/ZrO_2-Chits nanocomposites demonstrated excellent biocompatibility and electrochemical behavior when AuNPs were directly synthesized on the surface of ZrO_2 nanoparticles in one-step procedure using a chitsosan as reducing agent. Anti-HCV was immobilized on this nanocomposite to fabricate the immunosensor. The secondary antibody was immobilized on AuNPs/SiO_2-Chits nanocomposite, which enhanced signal response of the HCV immunosensor by accelerating the electron transfer between $[Fe(CN)_6]^{3-/4-}$ and electrode surface. Under optimized conditions, this immunosensor exhibited board liner range, good stability and high sensitivity for the detection of HCV core antigen. The assay was convenient and cost-effective, which provided a promising potential in the early diagnosis of HCV infection in clinical.

Acknowledgments This work was financially supported by National Natural Science Foundation of China (81171415), Natural Science Foundation of Chongqing, China (2010BB5356), and Foundation of

National Key Discipline in Laboratory Medicine, Chongqing Medical University, China (2010103).

References

1. Choo QL, Kuo G, Weiner AJ, Overby LR, Bradley DW, Houghton M (1989) Isolation of a cDNA clone derived from a blood-borne non-A, non-B viral hepatitis genome. Science 244:359–362. doi:10.1126/science.2496467
2. Nunes D, Fleming C, Offner G, Craven D, Fix O, Heeren T, Koziel MJ, Graham C, Tumilty S, Skolnik P, Stuver S, Horsburgh CR, Cotton D (2010) Noninvasive markers of liver fibrosis are highly predictive of liver-related death in a cohort of HCV-infected individuals with and without HIV infection. Am J Gastroenterol 105:1346–1353. doi:10.1038/ajg.2009.746
3. Gao M, Nettles RE, Belema M, Snyder LB, Nguyen VN, Fridell RA, Serrano-Wu MH, Langley DR, Sun JH, OBoyle DR II, Lemm JA, Wang CF, Knipe JO, Chien C, Colonno RJ, Grasela DM, Meanwell NA, Hamann LG (2010) Chemical genetics strategy identifies an HCV NS5A inhibitor with a potent clinical effect. Nature 465:96–100. doi:10.1038/nature08960
4. Grebely J, Mattews GV, Dore GJ (2011) Treatment of acute HCV infection. Nat Rev Gastro Hepat 8:265–274. doi:10.1038/nrgastro.2011.32
5. Strader DB, Wright T, Thomas DL, Seeff LB (2004) Diagnosis, management, and treatment of hepatitis C. Hepatology 39:1147–1171. doi:10.1002/hep.20119
6. Morota K, Fujinami R, Kinukawa H, Machida TJ, Ohno K, Saegusa H, Takeda K (2009) A new sensitive and automated chemiluminescent microparticle immunoassay for quantitative determination of hepatitis C virus core antigen. J Virol Methods 157:8–14. doi:10.1016/j.jviromet.2008.12.009
7. Hofmann WP, Dries V, Herrmann E, Gartner B, Zeuzem S, Sarrazin C (2005) Comparison of transcription mediated amplification (TMA) and reverse transcription polymerase chain reaction (RT-PCR) for detection of hepatitis C virus RNA in liver tissue. J Clin Virol 32:289–293. doi:10.1016/j.jcv.2004.08.011
8. Lee S, Kim YS, Jo MJ, Jin M, Lee DK, Kim S (2007) Chip-based detection of hepatitis C virus using RNA aptamers that specifically bind to HCV core antigen. Biochem Bioph Res Co 358:47–52. doi:10.1016/j.bbrc.2007.04.057
9. Alias MB, Patel K, Dahari H, Beaucourt S, Larderie P, Blatt L, Hezode C, Picchio G, Dhumeaux D, Neumann AU, McHutchison JG, Pawlotsky JM (2002) Clinical utility of total HCV core antigen quantification: a new indirect marker of HCV replication. Hepatology 36:211–218. doi:10.1053/jhep.2002.34130
10. Gaudy C, Thevenas C, Tichet J, Mariotte N, Goudeau A, Dubois F (2005) Usefulness of the hepatitis C virus core antigen assay for screening of a population undergoing routine medical checkup. J Clin Microbiol 43:1722–1726. doi:10.1128/JCM
11. Zanetti AR, Romano L, Brunetto M, Colombo M, Bellati G, Tackney C (2003) Total HCV core antigen assays: a new marker of hepatitis C viremia for monitoring the progress of therapy. J Med Virol 70:27–30. doi:10.1002/jmv.10355
12. Tanaka N, Moriya K, Kiyosawa K, Koike K, Aoyama T (2008) Hepatitis C virus core protein induces spontaneous and persistent activation of peroxisome proliferator-activated receptor a in transgenic mice: Implications for HCV-associated hepatocarcinogenesis. Int J Cancer 122:124–131. doi:10.1002/ijc.23056
13. Moscato GA, Giannelli G, Grandi B, Pieri D, Marsi O, Guarducci I, Batini I, Altomare E, Antonaci S, Capria A, Pellegrini G, Sacco R (2011) Quantitative determination of hepatitis C core antigen in therapy monitoring for chronic hepatitis C virus. J Virol Methods 54:61–65. doi:10.1159/000318878
14. Krishnadasa DK, Li W, Kumar R, Tyrrell DL, Agrawal B (2009) HCV-core and NS3 antigens play disparate role in inducing regulatory or effector T cells in vivo: Implications for viral persistence or clearance. Vaccine 28:2104–2114. doi:10.1016/j.vaccine.2009.12.037
15. Tang DP, Yuan R, Chai YQ (2008) Ultrasensitive electrochemical immunosensor for clinical immunoassay using thionine-doped magnetic gold nanospheres as labels and horseradish peroxidase as enhancer. Anal Chem 80:1582–1588. doi:10.1021/ac702217m
16. Lu LS, Liu B, Li SF, Zhang W, Xie GM (2011) Improved electrochemical immunosensor for myeloperoxidase in human serum based on nanogold/cerium dioxide-BMIMPF/l-Cysteine composite film. Colloids Surf B 86:339–344. doi:10.1016/j.colsurfb.2011.04.017
17. Yin ZJ, Wu JJ, Yang ZS (2010) A sensitive mercury (II) sensor based on CuO nanoshuttles/ poly(thionine)modified glassy carbon electrode. Microchim Acta 170:307–312. doi:10.1007/s00604-010-0359-4
18. Wang LY, Sun Y, Wang J, Wang J, Yu AM, Zhang HQ, Song DQ (2011) Preparation of surface plasmon resonance biosensor based on magnetic core/shell Fe_3O_4/SiO_2 and $Fe_3O_4/Ag/SiO_2$ nanoparticles. Colloids Surf B 84:484–490. doi:10.1016/j.colsurfb.2011.02.003
19. Dobson KD, McQuillan AJ (1997) An infrared spectroscopic study of carbonate adsorption to zirconium dioxide sol-gel films from aqueous solutions. Langmuir 13:3392–3396. doi:10.1021/la962024i
20. Gan N, Yang X, Xie DH, Wu YZ, Wen WG (2010) A disposable organophosphorus pesticides enzyme biosensor based on magnetic composite nano-particles modified screen printed carbon electrode. Sensors 10:625–638. doi:10.3390/s100100625
21. Klimova T, Rojas ML, Castillo P, Cuevas R, Ramirez J (1998) Characterization of Al_2O_3-ZrO_2 mixed oxide catalytic supports prepared by the sol-gel method. Micropor Mesopor Mat 20:293–306. doi:10.1016/s1387-1811(97)00024-3
22. Wang M, Li ZY (2008) Nano-composite ZrO_2/Au film electrode for voltammetric detection of parathion. Sens Actuat B 133:607–612. doi:10.1016/j.snb.2008.03.023
23. Zhang W, Yang T, Jiang C, Jiao K (2008) DNA hybridization and phosphinothricin acetyl-transferase gene sequence detection based on zirconia/nanogold film modified electrode. Appl Surf Sci 254:4750–4756. doi:10.1016/j.apsusc.2008.01.102
24. Huang HZ, Yang XR (2004) Synthesis of chitosan-stabilized gold nanoparticles in the absenc-e/presence of tripolyphosphate. Biomacromolecules 5:2340–2346. doi:10.1021/bm0497116
25. Jiang HJ, Zhao Y, Yang H, Akins DL (2008) Synthesis and electrochemical properties of single-walled carbon nanotube–gold nanoparticle composites. Mater Chem Phys 114:879–883. doi:10.1016/j.matchemphys.2008.10.075
26. Huang KJ, Niu DJ, Xie WZ, Wang W (2009) A disposable electrochemical immunosensor for carcinoembryonic antigen based on nano-Au/multi-walled carbon nanotubes–chitosans nanocomposite film modified glassy carbon electrode. Anal Chim Acta 659:102–108. doi:10.1016/j.aca.2009.11.023
27. Wang B, Chen K, Jiang S, Reincke F, Tong WJ, Wang DY, Gao CY (2006) Chitosan-Mediated Synthesis of Gold Nanoparticles on Patterned Poly(dimethylsiloxane) Surfaces. Biomacromolecules 7:1203–1209. doi:10.1021/bm060030f
28. Wang LL, Jia XE, Zhou YP, Xie QJ, Yao SZ (2010) Sandwich-type amperometric immuno-sensor for human immunoglobulin G using antibody-adsorbed Au/SiO_2 nanoparticles. Microchim Acta 168:245–251. doi:10.1007/s00604-009-0281-9
29. Tang J, Tang DP, Su BL, Li QF, Qiu B, Chen GN (2011) Nanosilver-penetrated polyion graphene complex membrane for mediator-free amperometric immunoassay of alpha-fetoprotein using nanosilver-coated silica nanoparticles. Electrochim Acta 56:3773–3780. doi:10.1016/j.electacta.2011.02.059
30. Lai GS, Wu J, Leng C, Ju HX, Yan F (2011) Disposable immunosensor array for ultrasensitive detection of tumor

markers using glucose oxidase-functionalized silica nanosphere tags. Biosens Bioelectron 26:3782–3787. doi:10.1016/j.bios.2011.02.032
31. Lin MH, Liu YJ, Liu CH, Yang ZH, Huang YB (2011) Sensitive immunosensor for benzo [a] pyrene detection based on dual amplification strategy of PAMAM dendrimer and amino-modified methylene blue/SiO_2 core–shell nanoparticles. Biosens Bioelectron 26:3761–3767. doi:10.1016/j.bios.2011.02.028
32. Li SF, Zhu XY, Zhang W, Xie GM, Feng WL (2011) Hydrogen peroxide biosensor based on gold nanoparticles/thionine/gold nanoparticles/multi-walled carbon nanotubes-chitosans composite film-modified electrode. Appl Surf Sci 258:2802–2807. doi:10.1016/j.apsusc.2011.10.138
33. Liu B, Lu LS, Li Q, Xie GM (2011) Disposable electrochemical immunosensor for myelo-peroxidase based on the indium tin oxide electrode modified with an ionic liquid composite film containing gold nanoparticles, poly(o-phenylenediamine) and carbon nanotubes. Microchim Acta 173:513–520. doi:10.1007/s00604-011-0575-6
34. Jiang HJ, Yang H, Akins DL (2008) Direct electrochemistry and electrocatalysis of catalase immobilized on a SWNT-nanocomposite film. J Electroanal Chem 623:181–186. doi:10.1016/j.jelechem.2008.07.024
35. Yang YH, Yang HF, Yang MH, Liu YL, Shen GL, Yu RQ (2004) Amperometric glucose biosensor based on a surface treated nanoporous ZrO_2/Chitosan composite film as immobilization matrix. Anal Chim Acta 525:213–220. doi:10.1016/j.aca.2004.07.071
36. Wang LY, Wang J, Zhang SL, Sun Y, Zhua XN, Cao YB, Wang XH, Zhang HQ, Song DQ (2009) Surface plasmon resonance biosensor based on water-soluble ZnO–Au nanocomposites. Anal Chim Acta 653:109–115. doi:10.1016/j.aca.2009.09.001
37. Liu XQ, Li BH, Wang X, Li CY (2010) One-step construction of an electrode modified with electrodeposited Au/SiO_2 nanoparticles, and its application to the determination of NADH and ethanol. Microchim Acta 171:399–405. doi:10.1007/s00604-010-0441-y
38. Lu LS, Liu B, Zhao ZH, Ma CX, Luo P, Liu CG, Xie GM (2011) Ultrasensitive electrochemical immunosensor for HE4 based on rolling circle amplification. Biosens Bioelectron 33:216–221. doi:10.1016/j.bios.2012.01.004
39. Qiu JD, Huang H, Liang RP (2011) Biocompatible and label-free amperometric immunosensor for hepatitis B surface antigen using a sensing film composed of poly (allylamine)-branched ferrocene and gold nanoparticles. Microchim Acta 174:97–105. doi:10.1007/s00604-011-0585-4
40. Mikawaa AY, Santosa SAT, Kenfea FR, Silvac FH, Costa PI (2009) Development of a rapid one-step immunochromatographic assay for HCV core antigen detection. J Virol Methods 158:160–164. doi:10.1016/j.jviromet.2009.02.013